A Transcriptionally Distinct Subpopulation of Healthy Acinar Cells Exhibit Features of Pancreatic Progenitors and PDAC

Vishaka Gopalan[1], Arashdeep Singh[1], Farid Rashidi Mehrabadi[1,2], Li Wang[3], Eytan Ruppin[1], H. Efsun Arda[3], and Sridhar Hannenhalli[1]

ABSTRACT

Pancreatic ductal adenocarcinoma (PDAC) tumors can originate either from acinar or ductal cells in the adult pancreas. We re-analyze multiple pancreas and PDAC single-cell RNA-seq datasets and find a subset of nonmalignant acinar cells, which we refer to as acinar edge (AE) cells, whose transcriptomes highly diverge from a typical acinar cell in each dataset. Genes upregulated among AE cells are enriched for transcriptomic signatures of pancreatic progenitors, acinar dedifferentiation, and several oncogenic programs. AE-upregulated genes are upregulated in human PDAC tumors, and consistently, their promoters are hypomethylated. High expression of these genes is associated with poor patient survival. The fraction of AE-like cells increases with age in healthy pancreatic tissue, which is not explained by clonal mutations, thus pointing to a nongenetic source of variation. The fraction of AE-like cells is also significantly higher in human pancreatitis samples. Finally, we find edge-like states in lung, liver, prostate, and colon tissues, suggesting that subpopulations of healthy cells across tissues can exist in preneoplastic states.

Significance: These findings show "edge" epithelial cell states with oncogenic transcriptional activity in human organs without oncogenic mutations. In the pancreas, the fraction of acinar cells increases with age.

Introduction

Pancreatic ductal adenocarcinoma (PDAC) is one of the deadliest cancers with approximately 8% survival rate at 5 years (1). Pathogenesis of PDAC, and in particular, the cell of origin for PDAC, is not yet fully resolved, thus impeding development of robust therapies. Recent work has demonstrated that in mice, PDAC tumors can be driven from both acinar and ductal cells (2), where an acinar to PDAC transformation is mediated by acinar–ductal metaplasia (ADM; ref. 3).

A classical view of cancer posits that oncogenesis is mediated by a series of somatic mutations in key oncogenes and tumor suppressors, accompanied by clonal selection (4, 5). Although this clonal genetic model is widely accepted as one of the dominant pathways to oncogenesis, epigenetic alterations also play a key role. Indeed, transcriptional and epigenetic heterogeneity in the progenitor cell population forms the basis for later malignant transformation (6), where such heterogeneity has been shown to be crucial for premalignant pancreatic lesions to progress to PDAC (7, 8). Furthermore, in a clonal cellular population, pervasive transcriptional fluctuation, in conjunction with complex regulatory networks, can result in a distinct meta-stable cellular state (9–11). For instance, in a clonal population of blood progenitors, high SCA1–expressing outlier cells preferentially commit to the myeloid lineage, whereas cells with low SCA1 expression commit to proerythrocytes (10). Taken together, this suggests a potential nongenetic basis for early stages of tumorigenesis, driven by transcription fluctuation across clonal cells, resulting in a distinct cell state primed for malignant transformation (11). Oncogenic mutations can further amplify this nongenetic heterogeneity, as seen in breast epithelial cell cultures where oncogenic mutations increase the rate of switching between nonstem and stem-like epithelial cells (12). An interplay between genetic and epigenetic alterations is likely to underlie complete malignant transformation (13).

In this work, we investigated the potential role of transcriptional heterogeneity in pancreatic epithelial cells in priming PDAC. We analyzed a published single-cell transcriptomic dataset comprising 57,730 cells from 24 PDAC tumors and 11 pancreas samples from patients having non-PDAC indications (14). We found that nonneoplastic acinar cells contained a subpopulation, which we refer to as edge cells (following the terminology in Li and colleagues; ref. 15), whose transcriptomes diverge from the average acinar cell and show features of premalignancy. In particular, genes that are differentially upregulated among the acinar edge (AE) cells are enriched for transcriptomic signatures of pancreatic progenitors and acinar dedifferentiation, as well as several oncogenic programs such as Kras signaling, fatty acid metabolism, and epithelial–mesenchymal transition (EMT). Furthermore, in human PDAC tumors, the genes upregulated in AE cells are upregulated and consistently, their promoters are hypomethylated. Higher expression of these genes also associates with PDAC patient survival. This suggests potential clinical relevance of these early malignancy priming events in acinar cells. Finally, we validate the existence of AE cells in additional independent pancreatic datasets and additionally find that the fraction of edge-like cells increases with age in healthy pancreatic tissue, thus providing a

[1]Cancer Data Science Laboratory, National Cancer Institute, Center for Cancer Research, National Institutes of Health, Bethesda, Maryland. [2]Department of Computer Science, Indiana University, Bloomington, Indiana. [3]Laboratory of Receptor Biology and Gene Expression, Center for Cancer Research, National Cancer Institute, National Institutes of Health, Bethesda, Maryland.

Corresponding Authors: Vishaka Gopalan, Cancer Data Science Laboratory, National Cancer Institute, Bethesda, MD 20814. Phone: 240-858-3577; E-mail: vishaka.gopalan@nih.gov; and Sridhar Hannenhalli, sridhar.hannenhalli@nih.gov

potential mechanism linking the known increase of PDAC incidence with age (1). Intriguingly, we see strong functional similarity between transcriptional drift from non-edge to edge acinar cells and those previously reported in healthy to premalignant lung transformation (16), suggesting that our observations in PDAC may possibly be more general. Indeed, we found edge-like cells to be significantly more prevalent in human pancreatitis samples, and furthermore, beyond the pancreas, we found edge-like states among epithelial cells in non-neoplastic lung, liver, prostate, and colon tissues.

Overall, our work suggests that transcriptional heterogeneity among nonmalignant epithelial cells may be large enough for a fraction to exist in a dedifferentiated, preneoplastic state. Because genes upregulated in this premalignant state also increased in expression with age, this may help explain the higher incidence rate of tumors with age in these tissues, in addition to other putative mechanisms associated with the increase in cancer risk with aging (17).

Materials and Methods

The code necessary for reproducing these results are available at https://github.com/hannenhalli-lab/pdac_edge. Details of data downloading and processing procedures are described in Supplementary Methods.

Two-stage statistical test for an edge subpopulation

Our procedure for testing whether a nonmalignant cell cluster harbors an edge subpopulation consisted of two tests—the skewness and the proximity tests.

Heterogeneity test

We selected the 1,000 most variable genes (using Seurat's default FindVariableFeatures function) in the nonmalignant cell cluster, z-score normalized their expression, and computed a 50-dimensional principal component (PC) embedding for each cell; we refer to these PCs as Normal PCs to underscore that they are computed only from the nonmalignant cell cluster. We then computed the distance of each cell from the cluster medoid based on Euclidean distance. The 10% of cells that are farthest from the medoid are termed outlier cells. We quantified heterogeneity as the skewness, s, of the distance distribution using the medcouple estimator from the robustbase package in R. To compute the statistical significance of s, we create 100 control cell clusters by shuffling each of the 50 Normal PC coordinates across all cells in the original cluster. For each control cluster, we compute the skewness as above, and based on a Gaussian fit of these 100 control skewness values, we estimated the empirical P value of s. We used a P value threshold of 0.05 to consider the cell cluster heterogeneous and proceed to the next test.

Proximity test

Here, we determine whether the outlier cells in the nonmalignant cluster are significantly closer to the malignant cell cluster than non-outlier cells. We carry out PCA jointly on both malignant cells and nonmalignant cells, using 1,000 most highly variable genes across these cells. We refer to these PCs as Pooled PCs. We then define the malignant cell cluster's medoid using the Euclidean distance metric, and compute the proximity ratio, R, as the ratio between the average distances of outlier cells (in the Pooled PC space) to the malignant cluster medoid to that of the non-outlier cells. A value of $R < 1$ implies that the outlier cells are closer to malignancy than non-outlier cells. We compute the statistical significance of R by randomly choosing 10% of the nonmalignant cells as outlier cells, and recompute R using these

control outlier cells. We repeat this process 100 times, fit a Gaussian to the obtained ratios and estimate the empirical P value of observing a value less than R. If this P value is less than 0.05, the outliers are labeled as edge cells.

Modified three-stage statistical test for finding edge heterogeneity

The three-stage pipeline retains the heterogeneity and proximity tests and incorporates a third collinearity test.

Heterogeneity test

We computed 5 Normal PCs based on the 1,000 most variably expressed genes within the nonmalignant cluster of interest. Using each PC individually, as above, we defined the medoid cell, computed the distance of each cell from the medoid, followed by skewness of the distance distribution, s, and its significance based on shuffling the expression separately among cells in each sample (this sample-aware shuffling removes any potential bias caused by inter-sample heterogeneity). The P values of s computed for all 5 PCs are corrected using the Benjamini–Hochberg FDR procedure. Each Normal PC with an FDR < 0.1 is chosen to define outlier cells, that is, 10% of cells farthest from the cluster medoid.

Proximity test

Five Pooled PCs are computed on the basis of the 1,000 most variably expressed genes across the pooled nonmalignant and malignant clusters. For each outlier cell population (defined by a particular Normal PC qualifying the Heterogeneity test), the proximity ratio of the outlier cells, R, and its P value, is computed separately for each pooled PC as above. The FDR is then computed for each pooled PC, and the set P of all Pooled PCs with an FDR < 0.1 are retained.

Collinearity test

We compute a 5×5 correlation matrix of Spearman correlation coefficient between every Normal and Pooled PC score pair across all cells in the nonmalignant cluster that qualify both heterogeneity and proximity tests. The P values of each correlation are corrected using the FDR method. For each skewed Normal PC, if there exists at least one collinear Pooled PC with a low proximity ratio (with a correlation FDR < 0.1), then the Normal PC is a direction of edge heterogeneity.

Gene set enrichment comparison with Mascaux and colleagues (16)

We divided the acinar cells into three bins based on their distances from the acinar medoid in PC space. We z-scored the normalized expression of each gene across all acinar cells and picked genes that increased in z-score by at least 0.1 between adjacent bins. We carried out a Fisher test for over-representation for 64 gene sets (50 Hallmark gene sets and 14 CancerSEA gene sets), after which, we carried out an FDR correction and picked gene sets with a q value of <0.1 as significant.

Motif enrichment and network analysis

To find a list of motifs enriched near acinar-expressed genes, we used the SPRY–SARUS motif scanner (18) to scan the central 100 bp region of ATAC-seq peaks for matches to motifs in the JASPAR 2020 vertebrate motif collection (19). Out of 746 motifs, we restricted our scans to 589 motifs that involved a transcription factor (TF) that was expressed in at least 10% of all acinar cells. We split the ATAC-seq peak regions into foreground or background sets depending on whether

or not the peaks were at most 10kb upstream of a gene expressed in at least one acinar cell. We scanned both sets of regions for motif matches ($P < 10^{-4}$) and carried out a Fisher test of over-representation among the foreground sequences for each motif. We then computed q values for each TF and retained TFs with a q value of <0.1.

For each retained enriched TF, we created gene sets that consisted of its putative gene targets in the foreground set. We scored each gene set's activity in each acinar cell using AUCell and used AUCell's internal Global_k1 threshold to declare a gene set as active or inactive in each acinar cell. We then computed the fraction of acinar cells in each of the 3 bins with an active gene set, with the same cell-bin assignment that was computed in **Fig. 2C**.

Variant calling

We called variants in acinar cells from the raw sequencing reads in GSE81547 and GSE85241 datasets using the GATK best practices workflow. We then removed variants that were (i) shared across donors, (ii) were annotated in dbSNP v138, (iii) had fewer than 5 reads aligning to the locus or had fewer than 3 reads supporting the alternate allele.

Comparing healthy tissue donors and cancer patient donors in Tosti and colleagues, 2021

Three of the samples—TUM-13, TUM-C1, and TUM-25—were derived from histologically normal pancreas locations in patients with cancer (neuroendocrine tumor, PDAC, and mixed Mullerian tumor, respectively). To verify that samples from patients with cancer did not possess higher edge gene set activity than healthy donors, we modeled edge gene set activity as a Gaussian linear mixed model with donor (random effect), sample type (healthy or tumor-adjacent, fixed effect), and cell type (random effect) as regressors. Because the effect of sample type on the edge gene set activity (coefficient = 0.0014, standard error = 0.016) was not statistically significant (t value = 0.089), we considered cells from both patients with cancer and healthy donors as normal.

Adaptive AUCell threshold computation

When running AUCell on the datasets analyzed in **Figs. 6** and **7**, we found that the AUCell Global_k1 threshold, which was computed after pooling all cells in a given study, was affected by variations in library sizes between cells collected from different donors. We thus developed an adaptive thresholding strategy where an activity threshold for the edge gene set was computed separately for each donor.

For a given donor, we generated a collection of expression-controlled gene sets containing the same number of genes as the edge gene set. We first divided all expressed genes in a donor into 10 bins based on their mean normalized expression and assigned each edge gene to a bin based on its normalized expression level. For each edge gene, we then picked a gene at random from the same expression bin. The activity of the resulting control gene set was then scored using AUCell, where the 95th percentile of the AUCell scores was stored as a putative activity threshold. This process was repeated 100 times, with the largest putative activity threshold chosen as the final edge gene set activity threshold. Any cell with an AUCell score higher than this threshold was considered to be an edge cell.

Survival analysis of The Cancer Genome Atlas patients with cancer

For each cancer type investigated here, we obtained the mRNA expression (in TPM units) and clinical data for The Cancer Genome Atlas (TCGA) patients with cancer from UCSC-xena browser (https://

xena.ucsc.edu/). We used Cox regression to model the overall survival of patients by using the median expression of each signature gene set (y-axis of **Fig. 3C**) as an explanatory variable. In addition, we used the age of patients as a covariate and stratified the model based on their gender to control for these potential confounders. The resulting P values were corrected for multiple comparisons using the FDR method and hazard ratios (HR) were plotted on log scale.

Expression analysis in bulk tumor data

For each cancer type investigated, we z-scored the expression of each gene in TCGA patients with cancer based on its mean and standard deviation in normal samples of corresponding tissue from GTEx and used the averaged z-scores to compare different gene sets. Before z-scoring, we performed quantile normalization to make the two datasets comparable.

DNA methylation analysis in bulk tumor data

We used 450k DNA methylation data of cancer and normal samples from array-expression for pancreas (20) and from GEO database for lung (GSE66836) and liver (GSE54503) samples. The coordinates of 450k methylation array probes were obtained using the COHCAP library in R and were mapped to the 5kb upstream promoter region of each gene using bedtools. We used the mean and standard deviation of aggregated methylation of each promoter in normal samples to compute the z-scores of the same in the cancer samples and plotted the averaged z-scores to compare different gene sets.

Results

Normal acinar cells include a transcriptionally divergent *edge* subpopulation shifted toward a malignant state

We obtained processed gene-wise read counts from RNA-seq profiling of 57,730 pre-annotated cells across 24 PDAC and 11 non-PDAC samples (14). The non-PDAC samples were taken from the normal pancreatic sites (Supplementary Table S1 in Peng and colleagues; ref. 14) of patients with other conditions: Neuroendocrine tumors ($n = 3$), solid pseudopapillary tumors ($n = 3$), serous cystic neoplasia ($n = 1$), mucinous cystic neoplasia ($n = 2$), duodenal intraepithelial neoplasia ($n = 1$), and small intestine papillary adeno-carcinoma ($n = 1$). We processed the data using Seurat v3.0 (21), following which, we used doubletFinder (22) to discard 2,877 potentially doublet cells, leaving us with 54,853 cells. These cells comprised 10 annotated types—T cells, B cells, macrophages, stellate cells, fibroblasts, endothelial cells, acinar cells, ductal cells (type 1 and 2) and endocrine cells. A UMAP plot of the data shows that the annotated cell types are well separated (Supplementary Fig. S1). In the original annotations of the data, ductal cell type 2 refers to malignant ductal cells, to contrast them with nonmalignant ductal cells (type 1).

If a given nonmalignant cell cluster, say X, passes the two statistical filters below, we state that X contains edge cells (**Fig. 1A**). The first filter—heterogeneity test—checks if a subset of cells in X have significantly diverged from X's medoid in PC space. These PCs, which we call Normal PCs, are computed on the basis of transcriptomes only in X to capture gene expression variation within X. If X passes the filter, we consider the 10% of cells farthest from X's medoid as candidate edge cells. The second filter—proximity test—checks if the candidate edge cells are significantly closer to the malignant cluster than the remaining cells in X. The proximity test is based on PC coordinates computed from cells in both X and the malignant cluster, which we call Pooled PCs. Technically, the heterogeneity test can also be carried out in Pooled
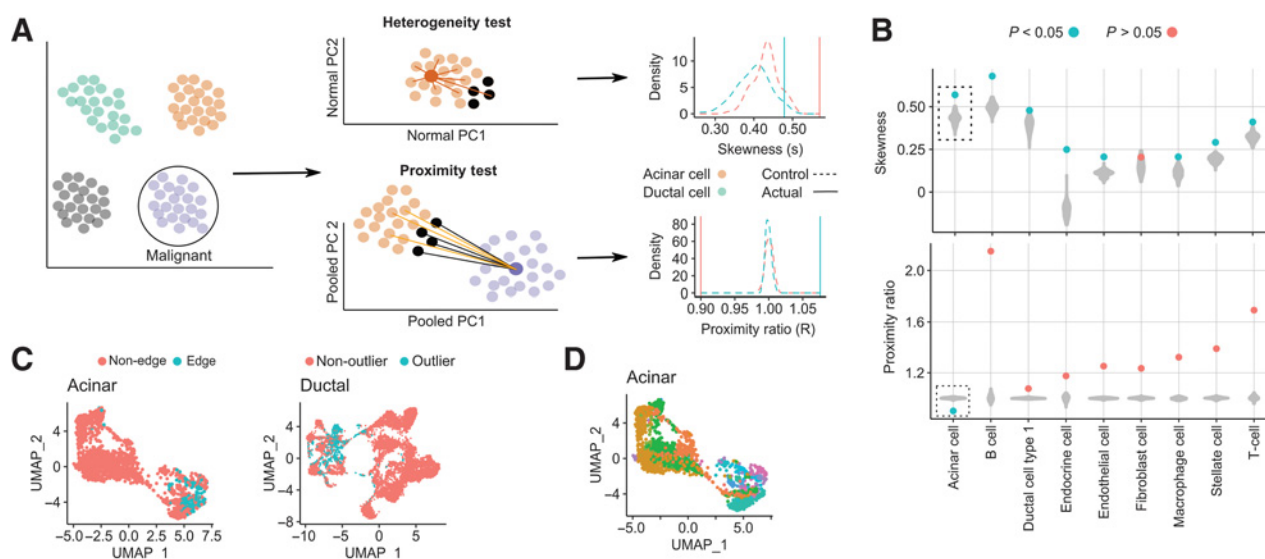
Figure 1.
Testing the presence of an edge subpopulation among nonmalignant cells in scRNA-seq data. **A,** Within each nonmalignant cluster, every cell's distance from the cluster medoid (in Normal PC space) was calculated, and the resulting distance distribution was tested for positive skewness. In the proximity test, we tested if the 10% of nonmalignant cells farthest from their own medoid (black, termed outlier cells) were significantly closer, in the Pooled PC space, to the malignant cluster medoid (dark purple) than the remaining 90% of cells (orange). If both test conditions held, the outlier cells were called edge cells. For both tests, examples of the distributions of skewness and the proximity ratio are shown for acinar and ductal cells, as well as their respective control populations. **B,** Violin plots of medoid distance distribution skewness values (top) and malignant proximity ratio (bottom) after shuffling were performed 100 times for each indicated cluster. Filled circles indicate skewness and proximity ratio values of actual cells, where blue and red indicate a significant (<0.05) or insignificant P value for each test. **C,** UMAP plots of edge and non-edge acinar cells (left) and non-outlier and outlier ductal cells (right). **D,** UMAP plots of acinar cells colored by their sample of origin (34 samples in total, as acinar cells from one sample were discarded as they were likely doublets).

PC space. However, because Pooled PCs also capture gene expression differences between X and the malignant cluster, they do not provide an unbiased measure of heterogeneity within X.

We assessed all 9 nonmalignant cell types and found that only acinar cells harbored edge cells, having uniquely passed both heterogeneity and proximity tests (**Fig. 1B**). The existence of edge cells in the acinar population is not due to copy-number alterations (CNA), as the acinar cells were shown not to harbor CNAs, compared with malignant ductal cells (14). The nonmalignant ductal cells passed the heterogeneity test but not the proximity test, suggesting that ductal cells are highly heterogeneous but that the candidate ductal edge cells (**Fig. 1C**) do not significantly drift toward malignancy. For clarity, we henceforth refer to the candidate edge ductal cells as outlier ductal cells.

We performed several controls (Supplementary Fig. S2A–S2E and Supplementary Section S1) to ensure that the AE population (**Fig. 1C** and **D**) did not arise from common artefacts related to single-cell sequencing such as cell cycle, inter-donor/batch variation, the presence of tumor-adjacent cells, and library size differences. Because our computational approach bears similarities to trajectory analysis, we also assessed an analogous trajectory-based pipeline based on Monocle3 (23) for detecting edge cells, where pseudotime values of cells were used for the heterogeneity and proximity tests. This alternative strategy (Supplementary Section S2), however, failed to detect edge cells.

Overall, these results reveal an edge subpopulation uniquely in non-neoplastic acinar cells that have transcriptionally drifted away from the acinar medoid and toward malignant ductal cells. In contrast, ductal cells possess an outlier ductal subpopulation that drift away from the ductal medoid but do not drift toward a malignant state.

Edge acinar cells diverge from a normal acinar phenotype and represent a preneoplastic state

Edge acinar cells expressed PRSS1, a marker of acinar cells, at much lower levels than non-edge acinar cells (Supplementary Fig. S2B, $P < 10^{-62}$). To further check whether edge acinar cells differentially expressed markers of dedifferentiation, we assessed the expression of genes curated by Baldan and colleagues (24) that are up- and down-regulated during acinar dedifferentiation. Four genes (*RBPJ, HNF1B, SOX9, MYC*) that are upregulated during dedifferentiation are also upregulated in edge acinar cells, whereas five genes (*AMY2A, RBPJL, SYCN, CPA1, CTRC*) that are downregulated during dedifferentiation are also downregulated in edge acinar cells (**Fig. 2A**). Acinar dedifferentiation precedes ADM—the conversion of acinar to ductal cells during pancreatic injury—that in turn is potentially a precursor to PDAC (25). We checked expression changes of the genes *STAT3, SEL1L, CBL, KLF4, CTNND1, ICAM1, DCLK1,* and *CDKN1A,* which are known to increase in expression during ADM (3). With the exception of *SEL1L*, all other genes were upregulated in edge acinar cells (**Fig. 2A**).

The acinar cell response during pancreatic injury has been suggested to represent a reversion to a multipotent embryonic pancreatic progenitor state (26), which, in mice embryos, is marked by expression of *Sox9, Ptf1a, Pdx1,* and *Nkx6–1* (27). We found that *SOX9* and *PDX1* were upregulated in edge acinar cells (**Fig. 2A**), although *NKX6–1* showed a negligible upregulation and *PTF1A* was downregulated. Nonetheless, we checked whether other genes active in pancreatic progenitors were also expressed in edge acinar cells by processing (see Supplementary Section S4 and Supplementary Fig. S2A and S2B) a single-cell RNA-seq dataset of human fetal (15.4 weeks gestational age) pancreatic tissue (28). We used AUCell (29) to score acinar and ductal
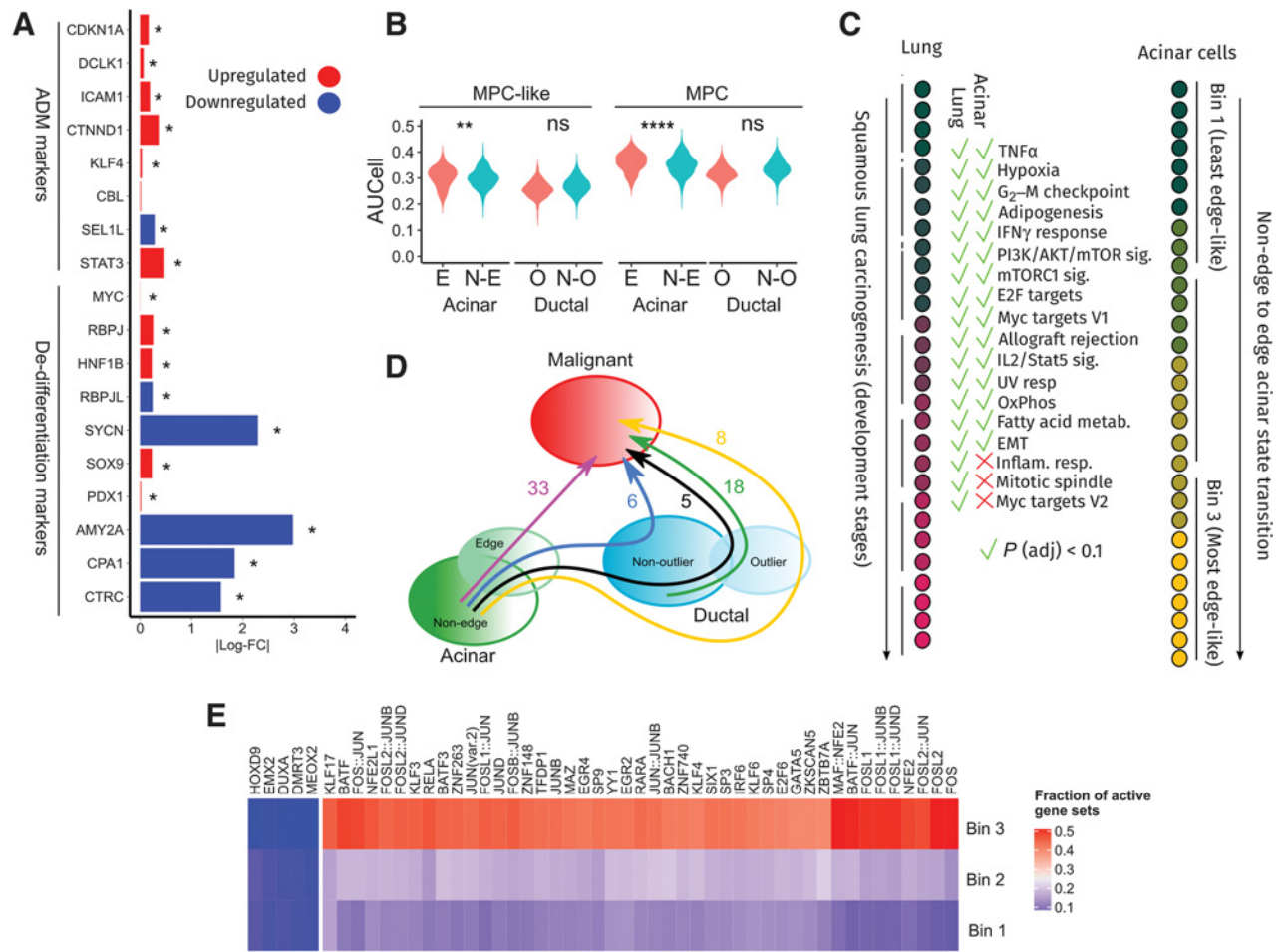
Figure 2.
Functional analysis of AE cells. **A,** Bars indicate log-fold changes between edge and non-edge acinar cells. **B,** The y-axis is the gene set activity, computed by AUCell, of multipotent cell (MPC) and multipotent cell-like (MPC-like) gene sets across cells in acinar and ductal cell subpopulations shown on the x-axis. ****, a P value less than 10^{-4}. **C,** Gene sets enriched among genes increasing monotonically in expression during lung cancer progression (left; ref. 16) and from Bin 1 to 3 of the non-edge to edge acinar transition (right). **D,** The number of oncogenic gene sets enriched among genes increasing in expression along the cell state transitions indicated by arrows. **E,** The fraction of acinar cells in each bin that have an active regulon of the TF indicated along the columns. These are the 50 most variably activated regulons across the three bins. ns, nonsignificant; *, $P < 0.01$; **, $P < 0.001$.

cells for the activity of genes that were upregulated in $SOX9^+PDX1^+$ multipotent cell (MPC)-like and $SOX9^+PTF1A^+NKX6{-}1^+PDX1^+$ MPC cells. Both gene sets were significantly more active in edge acinar cells than non-edge acinar cells (**Fig. 2B**), but not in outlier ductal cells when compared with non-outlier cells.

Because edge acinar cells are transcriptionally closer to malignant ductal cells than non-edge cells, we checked whether the non-edge to edge transition involved known pathways of tumorigenesis. To interpolate intermediate states between non-edge and edge states, we divided acinar cells into three equal-sized bins based on their distance from the acinar cluster medoid. We tested genes monotonically increasing expression across these bins for enrichment of genes from 50 Hallmark gene sets and 14 gene sets from the CancerSEA (30) database. Out of 19,276 genes expressed in acinar cells, 3,273 genes exhibited a monotonic increase in expression from the first to the third bin and were enriched for 43 of the 64 gene sets ($q < 0.1$; Supplementary Table S1). 15 of these gene sets overlapped with gene sets enriched among genes increasing in expression across early stages of lung malignant transformation documented in Mascaux and colleagues

(**Fig. 2C**; ref. 16), including genes related to Myc targets, mTOR signaling, IL2 STAT5 signaling, TNF-alpha signaling via NFKB, response to IFN-gamma, EMT, and UV response.

Next, we investigated four potential paths between non-outlier acinar to malignant cell states (**Fig. 2D**). We identified the genes monotonically increasing in expression along each of these paths and identified enriched oncogenic pathways (Supplementary Fig. S3C) among these genes. We observed most oncogenic changes (33 pathways enriched) along the path "non-edge acinar → edge acinar → malignant" (**Fig. 2D**). We contrasted this with two other paths, namely, "non-edge → edge → outlier ductal → malignant" and "non-edge → edge → all ductal cells → malignant," where, respectively, only 8 and 5 pathways were enriched. This contrast suggests that ductal cells may not always be an intermediate transition state between edge acinar and malignant ductal cells.

Next, leveraging TF motifs and acinar-specific ATAC-seq data (31), we analyzed TF activity in each of the three acinar cell bins to understand the transcriptional networks potentially driving the edge acinar state (see Supplementary Section S4). We focused on the 50 TFs
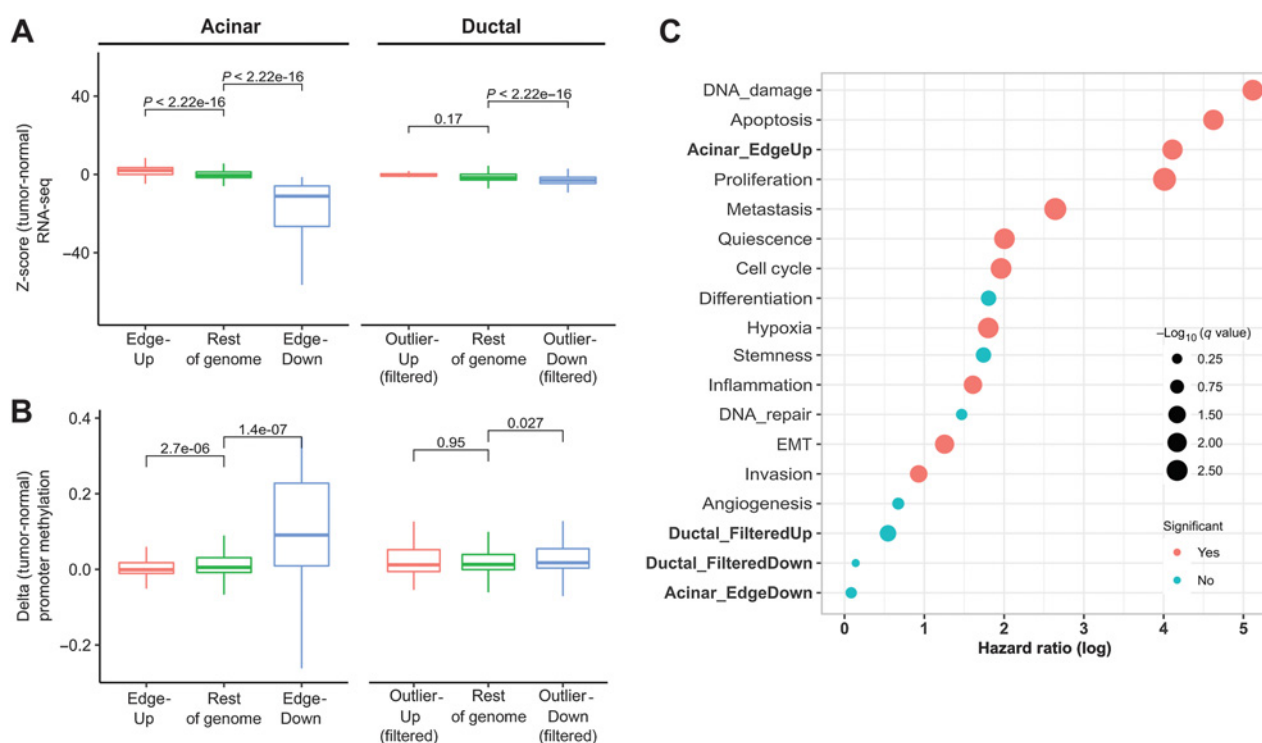
Figure 3.
AE and ductal outlier genes in TCGA PDAC. **A,** RNA-seq expression z-scores in PDAC samples (using GTEx pancreas RNA-seq as a reference) of upregulated (red), downregulated (blue), and remaining (green) genes in edge acinar cells and outlier-ductal cells. Genes in the Outlier-Up and Outlier-Down datasets were filtered to remove overlapping Edge-Up and Edge-Down genes. **B,** Methylation z-scores among PDAC using methylation samples from healthy samples as a reference (see Materials and Methods) of gene promoters in **A**. **C,** Log of HRs obtained from Cox regression of gene sets in TCGA PDAC samples.

whose putative target gene sets showed the most variable activity among all bins (**Fig. 2E**, see Supplementary Table S2 for a complete table of all 230 TFs). The *RBPJ* gene set showed high activity in Bin 3, which, along with the increase in *RBPJ* expression in edge acinar cells, provides a putative mechanistic link to the re-activation of embryonic progenitor genes in edge acinar cells (32). The activity of several *KLF* factors increased in Bin 3, including *KLF5*, whose knockout is known to reduce proliferation in low-grade PanIN cell lines (33). *HES1* activity, which maintains acinar plasticity (34), also increased from Bin 1 to 3.

Thus, edge acinar cells differentially upregulate markers of acinar dedifferentiation and ADM, and reactivate genes expressed in embryonic pancreas progenitor cells. This is concomitant with the activation of several oncogenic processes, driven by key TFs, during transition from a non-edge to edge acinar cell state. More surprisingly, there is a substantial commonality between the processes upregulated in transition from a non-edge to edge acinar cell state and those upregulated during lung premalignant progression.

Genes upregulated in edge acinar cells are predictive of PDAC survival

We created gene sets consisting of genes significantly upregulated and downregulated in edge acinar cells (Edge-Up and Edge-Down, Supplementary Table S3) and outlier ductal cells (Outlier-Up and Outlier-Down), compared with their respective non-edge and non-outlier counterparts, and analyzed their RNA-seq expression and promoter methylation in both healthy pancreatic tissues and human PDAC tumor samples. We found that Edge-Up genes were upregu-

lated, whereas Edge-Down genes were downregulated in PDAC tumors from the TCGA database, compared with healthy pancreatic tissues from the GTEx database (**Fig. 3A**). Consistent with gene expression, we found significant hypomethylation at promoters of Edge-Up and hypermethylation of Edge-Down gene promoters in PDAC samples (**Fig. 3B**). This suggests that gene expression and methylation changes in AE cells foreshadow changes in PDAC tumors in a consistent manner.

When we repeat these analyses for ductal Outlier-Up and Outlier-Down gene sets, counterintuitively (because outlier ductal cells do not exhibit a drift toward malignancy), we found a similar trend as for ductal cells, where Outlier-Up genes were upregulated whereas Outlier-Down genes were downregulated in PDAC tumors (Supplementary Fig. S3E), and Outlier-Up gene promoters were hypomethylated (**Fig. 3B**), though Outlier-Down gene promoters were not hypermethylated. We scrutinized these counter-intuitive observations and found that this is likely because over half the Outlier-Up genes were also Edge-Up genes, with only 8 Outlier-Up (and 177 Outlier-Down genes) being ductal-specific in their expression pattern. Removal of these overlapping genes eliminates these trends in RNA-seq and methylation patterns (**Fig. 3A** and **B**).

We further assessed, using a Cox proportional-hazards model, whether the four gene sets' activity in PDAC tumors are associated with patient survival. As shown in **Fig. 3C** and Supplementary Fig. S3E, both Edge-Up and Outlier-Up gene sets have a significant HR ($q < 0.1$), but Edge-Up gene set has a higher HR than Outlier-Up genes. Notably, neither Edge-Down nor Outlier-Down gene sets are significantly associated with survival. As above, repeating the survival analysis
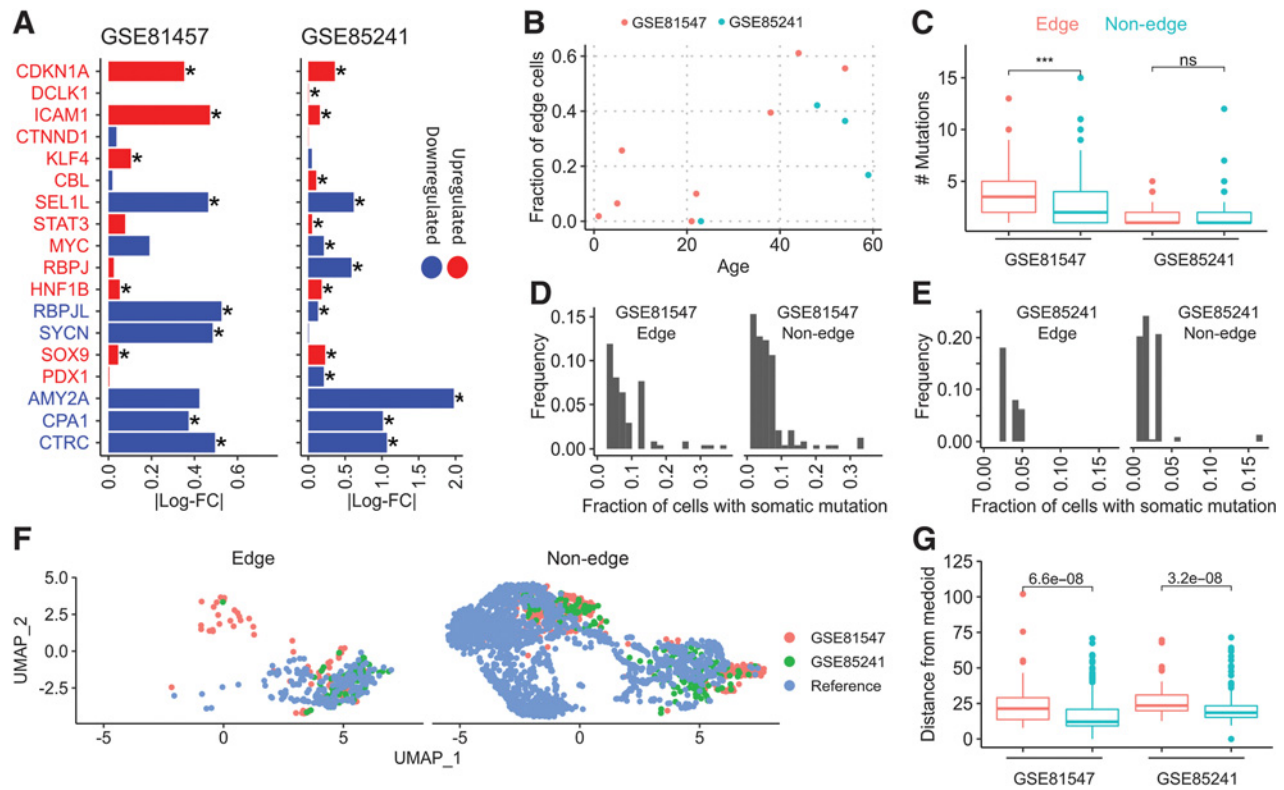
Figure 4.
AE cells in independent datasets and links with aging. **A,** Bars indicate log-fold changes between edge and non-edge acinar cells in GSE81547 and GSE85241. Markers in red and blue fonts are known to be upregulated and downregulated, respectively, during ADM (*CDKN1A* to *STAT3*) and dedifferentiation (*MYC* to *CTRC*). Matching color of the marker text and the bar indicates that the observed log-fold change matches the expected gene expression change of the marker. **B,** Scatter plot of fraction of edge acinar cells with tissue donor age. **C,** Number of mutations in edge and non-edge acinar cells. **D** and **E,** Histogram of the fraction of edge and non-edge cells that contain a somatic mutation. **F,** UMAP of acinar cells from GSE81547, GSE85241, and the reference dataset (14). **G,** Distance of edge (red) and non-edge (cyan) cells from the medoid acinar cell in PCA space computed separately for each dataset. ns, nonsignificant; *, $P < 0.01$; ***, $P < 0.0001$.

based on ductal-specific Outlier-Up genes does not show significant association with survival. We also performed Cox regression for oncogenic gene sets in CancerSEA and found that a majority of these sets were predictive of survival, albeit with a lower HR than the Edge-Up gene set.

These results suggest that the genes increasing in expression in the edge acinar state were key to tumor progression and are in line with our findings (**Fig. 2C**) that several oncogenic processes are enriched only among genes increasing in expression during the non-edge to edge transformation.

AE cells are found in independent healthy pancreas samples

We checked whether edge states can be found among acinar cells in other published single-cell datasets of human pancreatic tissues. We re-analyzed published SMART-seq (GSE81547; ref. 27) and CEL-seq (GSE85241; ref. 35) single-cell RNA-seq datasets of healthy human pancreas samples from donors spanning four decades of age. We removed genes that showed an age-associated increase in expression from our edge signature (see Supplementary Section S4) and used AUCell to score edge gene set activity in both datasets separately. Cells were declared as edge or non-edge based on the Global_k1 activity threshold computed by AUCell. First, similar to **Fig. 2A**, we compared the log-fold changes of ADM and acinar dedifferentiation markers

between edge and non-edge acinar cells (**Fig. 4A**). In GSE81547, all 9 dedifferentiation markers, and 6 out of 9 ADM markers, showed consistent fold-changes with edge acinar cells. In GSE85241, 6 out of 9 dedifferentiation markers, and 4 out of 9 ADM markers, showed consistent fold-changes with edge acinar cells.

Consistent with PDAC risk increases with age, we found an age-dependent increase in the fraction of edge cells ($R^2 = 0.66$, $P = 0.02$) across both datasets (**Fig. 4B**). As tissues accumulate somatic mutations during aging, we assessed whether edge cells possessed somatic, especially oncogenic, mutations, using the GATK pipeline (see Materials and Methods). The number of somatic mutations in these cells agreed with estimates of somatic mutations rates in pancreas tissue in GTEx data (36). We found that edge acinar cells had more somatic mutations than non-edge acinar cells in GSE81547 but not in GSE85241 (**Fig. 4C**). The differences between both datasets likely stem from differences in their library sizes, with GSE81547 being sequenced to a much higher depth (37). Nonetheless, in both datasets, all these mutations were rare, and were present, on average, in 2.18% and 3.47% of non-edge and edge cells in GSE85241, and in 6.34% and 8.53% of edge cells, respectively, in GSE81547 (**Fig. 4D** and **E**), which does not support a clonal origin for edge cells. This modest difference in mutation frequency between edge and non-edge cells was not significant based on

sampling that preserves the number of edge and non-edge cells in each sample. Furthermore, none of the mutations in edge and non-edge cells were classified as oncogenic driver mutations in the COSMIC cancer gene census (v92; ref. 38).

We compared the edge cells from these two datasets with the edge cells found in our reference dataset. After batch-correction, edge and non-edge cells overlapped each other in UMAP space (**Fig. 4F**), and edge cells in GSE81547 and GSE85241 were significantly farther from their medoid than non-edge cells (**Fig. 4G**). Thus, the edge states in each of these datasets are similar and represent a transcriptional drift away from the normal acinar state in each of them.

These findings validate the existence of edge-like acinar subpopulation cells in additional datasets, where they consistently exhibit expression profiles of ADM and dedifferentiation markers as in the PDAC dataset. Furthermore, we observe a strong correlation between frequency of edge cells and age.

Edge-like variation in other tissues

Alveolar type 2 (AT2) cells are believed to be the cell-of-origin (39) of lung adenocarcinoma (LUAD) tumors. However, application of our original pipeline on scRNA-seq data from nonmalignant (AT2) and LUAD samples (40) did not detect an edge subpopulation among AT2 cells, or any other nonmalignant lung epithelial cluster. We then modified our original pipeline to check whether any individual PCs reflected significant gene expression heterogeneity and a drift toward malignancy. Here, heterogeneity and the proximity tests are done for individual Normal and Pooled PCs respectively, and an additional test of collinearity between the quali-

fying Normal PC and the qualifying Pooled PCs (**Fig. 5A**, Materials and Methods). We note that multiple Normal PCs can show heterogeneity and drifts toward malignancy, reflecting the activation and inhibition of different gene sets in a subset of nonmalignant cells. With this refined pipeline, we found that Normal PC5 of AT2 cells defined an edge population that showed a drift toward a malignant cell cluster (Tumor State 2) along Pooled PC 1, which is collinear with Normal PC5 (Correlation coefficient = 0.82, $q < 10^{-9}$). In addition, Normal PC1 of Club cells, and Normal PCs 1 and 2 of AT1 cells, also represented drifts toward malignancy.

We then tested our pipeline on nonmalignant liver (caveats with this dataset discussed in Supplementary Section S3; refs. 41, 42), colon (43, 44), and prostate tissues (45) to find edge subpopulations that showed a drift toward liver hepatocellular carcinoma, colorectal cancer, and prostate adenocarcinoma, respectively. We found multiple clusters in each dataset that showed a drift toward malignancy in each of these tissues, including two hepatocyte clusters (Hep2 and Hep3) in the liver, transit-amplifying cells (TA1 and TA2), enterocytes, enterocyte progenitors, and intestinal stem cell clusters in the colon, and basal and luminal cells in the prostate. Genes upregulated in the edge-like populations in these tissues were enriched for several oncogenic gene sets (Supplementary Fig. S3D). Edge-like AT2 and AT1 cells in the lung, and TA1 (Transit Amplifying) cells in the colon, were enriched (Fisher test, $P = 0.042$, $P = 0.05$, and $P = 0.027$, respectively) for gene sets active in lung cancer progression in the Mascaux and colleagues study (**Fig. 5B**; ref. 16).

Overall, although we did not find a global transcriptomic shift toward malignancy in lung, liver, prostate, and colon, our results
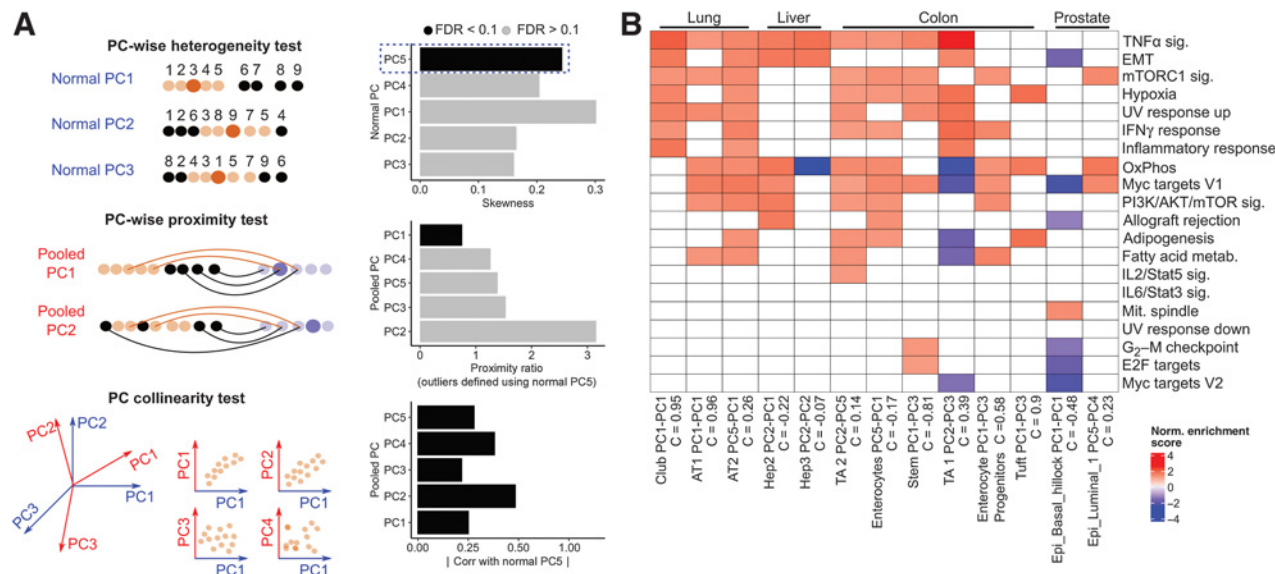
Figure 5.
Edge heterogeneity in epithelial cells of lung, liver, prostate, and colon. **A,** Schematic of three-stage pipeline to detect directions of edge heterogeneity. Each Normal PC was tested for positive skewness, and each PC that passed the test was used to define an outlier cell population (black). For each outlier population, each Pooled PC was then used to compute distances between non-neoplastic and malignant cells and carried out the proximity test, with all PCs tested for collinearity with the Normal PC used to define the outlier cells. Collinearity is defined as the Spearman correlation between the Normal and Pooled PC scores of all non-neoplastic cells in the cluster. Those skewed Normal PCs that were collinear (FDR < 0.1) with a Pooled PC that passed the proximity test represent directions of edge heterogeneity within the non-neoplastic cluster. The bar plots shown are from running the three-stage test on alveolar type 2 (AT2) cells, where Normal PC 5 was used to define outlier cells. **B,** Normalized enrichment scores of gene sets (those that were active during lung cancer progression in Mascaux and colleagues; ref. 16) enriched in indicated edge-like populations. The Normal and Pooled PC pair that passed heterogeneity and proximity ratio tests, along with their collinearity scores (which had $q < 0.1$) are shown.
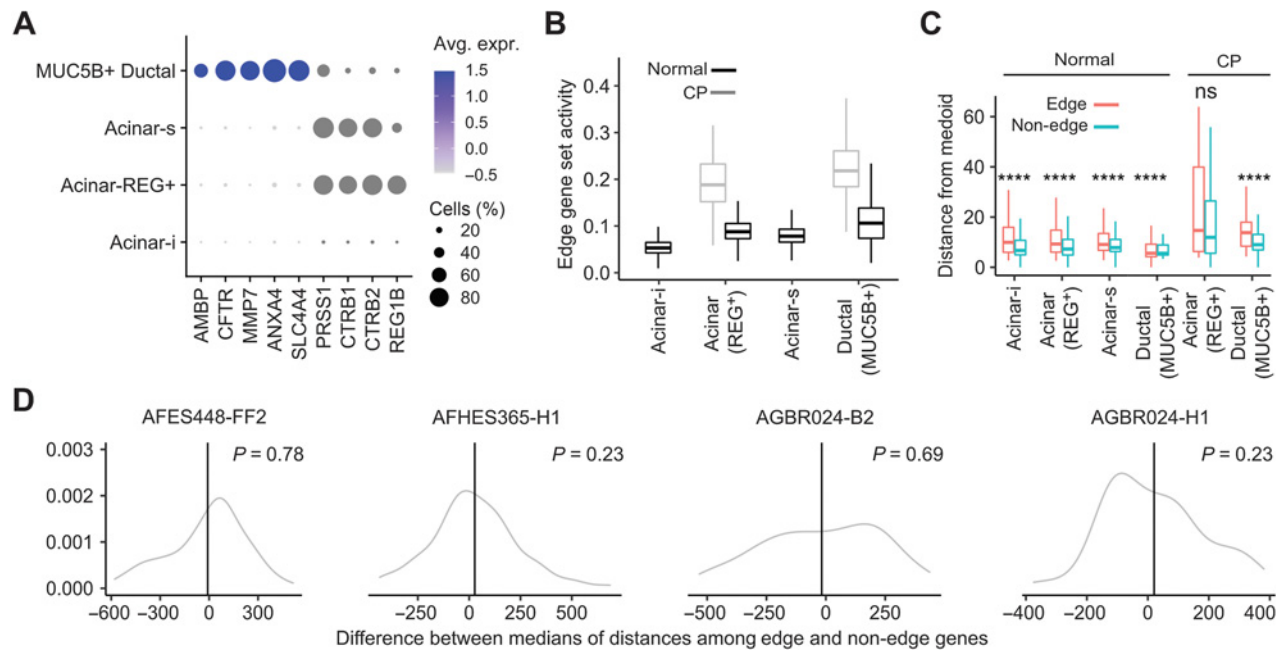
Figure 6.
Analysis of single-nucleus RNA-seq and spatial transcriptomic data from healthy and chronic pancreatitis samples. **A,** Expression of ductal marker genes (*AMBP, CFTR, MMP7, ANXA4*) and acinar marker genes (*PRSS1, CTRB1, CTRB2, REG1B*) in acinar subtypes and *MUC5B*^{+} ductal cells. **B,** Activity of the edge gene set across acinar subtypes and *MUC5B*^{+} ductal cells in normal and chronic pancreatitis (CP) biopsies. There were no Acinar-i and Acinar-s cells in the chronic pancreatitis biopsy. **C,** Euclidean distance of edge and non-edge cells, identified using an independently ascertained signature, from the medoid of pooled acinar and *MUC5B*^{+} ductal cells in PCA space. **D,** Distributions (gray) of the difference between the median interpixel distances among randomly chosen edge genes on the one hand and non-edge genes on the other in different healthy donors (donor ID shown in panel titles). Vertical black lines are the corresponding difference between median interpixel distances among actual edge and non-edge genes. One-sided *P* values were computed from a Gaussian approximation to the distribution shown in gray. ns, nonsignificant; ****, *P* < 0.00001.

suggest significant heterogeneity in specific oncogenic programs in multiple epithelial clusters in these tissues.

The edge acinar state is activated during chronic pancreatitis

Pancreatitis is associated with an increased PDAC risk (46). To investigate whether the increased risk is associated with the presence of edge cells, we analyzed a single-nucleus RNA-seq dataset of 120,000 cells in pancreas samples from healthy donors, patients with chronic pancreatitis, and histologically normal tissues adjacent to pancreatic tumors (47). In addition to reporting three acinar cell states (Acinar-i, Acinar-s and Acinar-*REG*[+]), the study had reported a novel *MUC5B*^{+} ductal population that also expressed acinar cell markers, where 45% of these cells expressed *PRSS1* (**Fig. 6A**). We used AUCell to compute edge gene set activity among the acinar and *MUC5B*^{+} ductal cells, and labeled cells as "edge" based on a more stringent and adaptive activity threshold (see Materials and Methods) than AUCell's Global_k1 threshold. The detected edge population was enriched for cells from the *MUC5B*^{+} ductal cell population (odds ratio = 4.962, *P* < 10[−116]), Acinar-*REG*[+] (odds ratio = 4.45, *P* < 10[−170]) and Acinar-s populations (odds ratio = 5.07, *P* < 10[−170]), but not the Acinar-i population (the odds ratio was relative to the expectation based on all acinar cells). Furthermore, relative to normal samples, acinar cells from chronic pancreatitis biopsies were over-represented in the edge population (odds ratio = 3.83, *P* < 10^{−66}), consistent with higher expression of the edge gene set in Acinar-*REG*[+] and *MUC5B*^{+} ductal cells in chronic pancreatitis biopsies (**Fig. 6B**). In addition, when we performed PCA separately for each cell type and donor type, we found that, by and large, edge cells were farther away from the medoid cell than non-edge cells (**Fig. 6C**).

Next, we checked whether any of the edge genes were detectable in the normal pancreas in histopathology data. *MMP7* was one of the highest upregulated genes in our edge gene set (Average Log-FC = 1.87), and is known to contribute to PDAC initiation and progression (48). Although *MMP7* expression occurs in PDAC cells (49), multiple studies reported that a small fraction of normal pancreatic samples showed low-antibody staining for *MMP7* (49–51). This observation is consistent with a small fraction of acinar cells in the healthy pancreas being in an edge state in some of the normal samples.

Finally, we evaluated the spatial localization of edge cells among spatial transcriptomic datasets assayed from a subset of healthy donors. These data were collected using the Cartana *in situ* sequencing platform, where pixel-wise locations of expression of each of 98 chosen genes were measured. We used the locations of 10 genes—nine from the edge gene set (*LCN2, CALD1, B2M, HLA-DRA, CD74, CD3D, KRT19, REG3G*), and *MUC5B*—as an indicator of the location of edge cells. We reasoned that, if edge cells exist in a single cluster, the distance between a given pair of pixels expressing an edge gene would, on average, be significantly shorter than that of a non-edge gene. We checked whether the median interpixel distance of each of the 10 edge genes was shorter than that of a random chosen set of 10 genes and found that this was not the case in any of the tissue slices (**Fig. 6D**). However, this does not preclude the possibility that the edge cells could exist as clusters at multiple foci distributed across the pancreas.
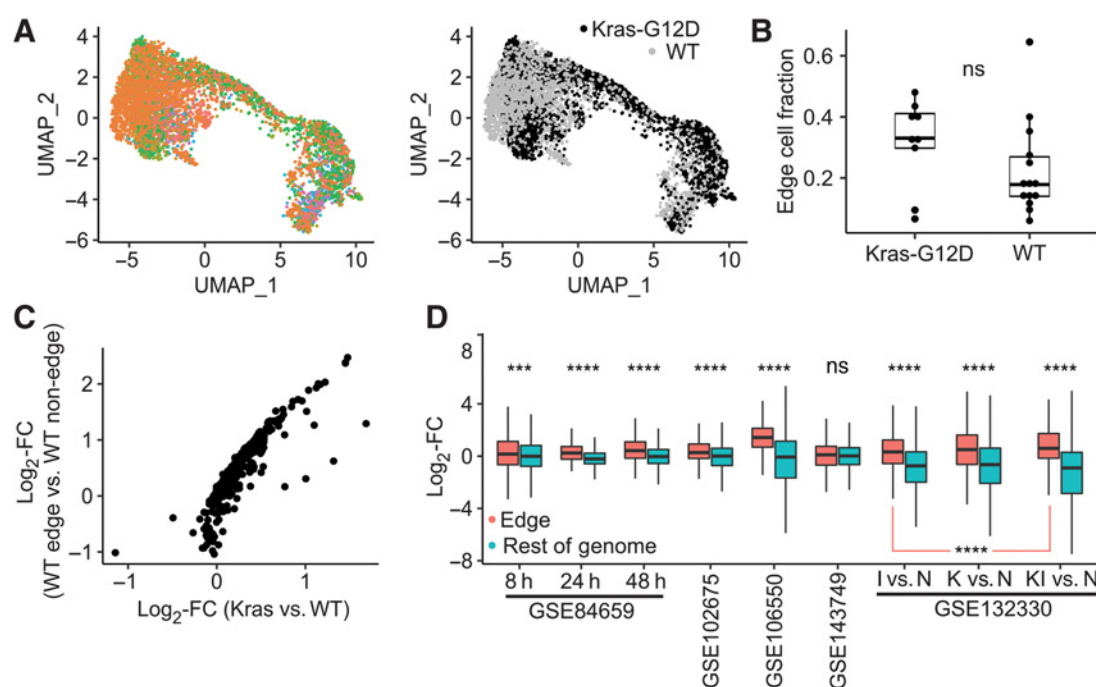
Figure 7.
Analysis of single-cell RNA-seq and bulk RNA-seq from healthy and Kras^{G12D}–bearing mice. **A,** UMAP plots of acinar cells from batch-integrated $Kras^{WT}$ and $Kras^{G12D}$ mice. Left, cells are colored according to batch. Right, cells are colored by Kras mutation status. **B,** Fraction of edge cells in $Kras^{G12D}$ mice and $Kras^{WT}$ mice. **C,** Average gene expression log-fold differences between acinar cells from $Kras^{G12D}$ mice and $Kras^{WT}$ mice (x-axis) and between edge and non-edge cells in $Kras^{WT}$ mice (y-axis). **D,** Log-fold changes of expression of edge genes (red) and non-edge genes (blue) observed in published studies where RNA-seq is carried out before and after pancreatitis is induced by caerulein treatment. ns, nonsignificant; ***, $P < 0.0001$; ****, $P < 0.00001$.

Kras mutations induce an edge-like transcriptional state in acinar cells in mice

KRAS is the most frequently mutated oncogene in human PDAC, and is mutated in nearly all PDAC samples in TCGA (52), with the $KRAS^{G12D}$ mutation believed to drive PDAC initiation. We checked whether $Kras^{G12D}$ mutation-bearing acinar cells in mice are more likely to be in an edge-like state by detecting them among pooled single-cell acinar transcriptomes (**Fig. 7A**) from $Kras^{WT}$ mice [from the Tabula Muris (53) and Tabula Muris Senis (54) projects] and from neoplastic PDAC lesions in Kras^{G12D}-bearing mice in the KIC model ($Kras^{LSL-G12D/+}Ink4a^{fl/fl}Ptf1a^{Cre/+}$, GSE125588; ref. 8) and the PRT mouse model (*Ptf1a-CreER, LSL-Kras^{G12D}, LSL-tdTomato*, GSE141017; ref. 55). We used AUCell (with an adaptive threshold) and mouse orthologs of the human edge gene set to detect edge cells and found that $Kras^{G12D}$ mice contained a larger fraction of edge acinar cells than $Kras^{WT}$ mice, although not at a statistically significant level ($W = 86$, Wilcoxon one-sided test, $P = 0.16$, **Fig. 7B**). Interestingly, we found a high correlation (Spearman rho = 0.88, $P < 2.2 \times 10^{-16}$, **Fig. 7C**) between log-fold changes in gene expression between edge and non-edge cells in $Kras^{WT}$ mice on the one hand with log-fold changes in gene expression between $Kras^{G12D}$ acinar cells and $Kras^{WT}$ acinar cells on the other. There is thus a large concordance between gene expression programs activated by the $Kras^{G12D}$ mutation and those activated during a non-edge to edge transition. Finally, we analyzed published bulk RNA-seq profiles of mouse pancreatic samples before and after pancreatitis induction (56–60). With the exception of GSE143749 (59), where log-fold changes were compared between pancreatic tuft and non-tuft cells, the edge gene set was more strongly upregulated than non-edge genes in the remaining pancre-

atitis samples (**Fig. 7D**). In particular, in GSE132330 (60), edge genes were more strongly upregulated after pancreatic injury in $Kras^{G12D}$ mice (KI vs. N) than in $Kras^{WT}$ mice (I vs. N, $P = 1.07 \times 10^{-5}$).

There is, thus, a clear concordance between gene expression changes during the non-edge to edge transition and those produced by $Kras^{G12D}$ induction and pancreatitis in mice.

Discussion

Here, we show the existence of a subset of nonmalignant acinar cells that we refer to as edge cells (15), which are transcriptionally distinct from a typical acinar cell, and significantly closer to malignant PDAC cells. This phenomenon is observed broadly across individuals and in multiple datasets. Although edge cells do not seem to be driven by clonal somatic mutations, interestingly, we see evidence of increased prevalence of edge cells with age, and consistently, an enrichment of edge-upregulated genes among genes increasing in expression with age. Our analysis of spatial transcriptomic data suggests that edge cells likely do not exist as a single cluster within the healthy pancreas, and are potentially distributed across the pancreas, either as isolated cells or in multiple clusters.

One way to interpret the observed global transcriptional drift in AE cells toward malignancy is that there are overlapping oncogenic programs that individually show heterogeneity in the non-malignant cell population, and are broadly concordant with each other. Ultimately, an increased transcriptional activity along multiple oncogenic programs in a subset of cells is revealed as the edge cells by our approach. Importantly, gene expression changes during the non-edge to edge transition are similar to those induced by the $Kras^{G12D}$

mutation and during pancreatitis. This suggests that the edge acinar state, which can be found even in histologically normal pancreas samples, is associated with, and possibly contributes to, both pancreatitis and PDAC. Furthermore, because the gene expression differences between edge and non-edge acinar cells in mice are similar to those induced by the $Kras^{G12D}$ mutation, it is possible that edge cells "pre-activate" a $Kras^{G12D}$-induced program that leads rapidly to oncogenesis upon mutation. Our results also reveal significant heterogeneity involving several oncogenic programs in nonmalignant epithelial cells of lung, liver, prostate, and colon.

There is a significant overlap between pathways activated in the non-edge to edge transitions in acinar cells on the one hand, and those activated during premalignant progression in the lung on the other. In AE cells, we see an upregulation of the targets of TFs *RBPJ, HES1*, and *KLF5* targets, which are known to mediate acinar cell plasticity and a reversion to a multipotent pancreatic progenitor state (32, 34). This suggests a role for known transcriptional networks playing a role in the transition to an edge state. In the context of regulatory networks, transcriptional fluctuations can lead to nongenetic phenotypic heterogeneity (9, 10, 61), which, in malignant cells, can lead to drug resistance (62) in a manner that can be perturbed by targeting key TFs (63).

The duration for which a cell remains in an edge state may involve epigenetic mechanisms like DNA methylation and histone modifications (64, 65). Coupled single-cell transcriptomics and DNA methylation data from the same acinar cell, which is needed to precisely assess the role of DNA methylation in sustaining the edge cell population, are currently not available. However, we found that the promoters of genes that are upregulated in the edge acinar cells relative to non-edge cells, were hypomethylated in PDAC tumors, and the converse was true for genes downregulated in edge acinar cells, suggesting a potential role of epigenetics in maintaining the edge cell state.

A potential role of the tissue environment, and DNA methylation, in giving rise to edge cells is further supported by our observed link between age and the fraction of edge cells in healthy acinar cells. Aging is the greatest risk factor for most cancers (66). Although clonal expansion of somatic mutations does occur with age in certain tissues such as skin and esophagus (67), we found no evidence of clonal expansion in the edge acinar cells. Beyond the role of mutations,

epigenetic changes from age-related hypomethylation (68) likely contribute to the stability and rate of switching to an edge state with age. Though we do not find mutations underlying the edge cells in the pancreas, the edge state may represent a state primed for malignant transformation by oncogenic mutation (13) or other age-associated transcriptomic changes (17, 69, 70)

Overall, our results support the notion of an edge transcriptomic state in healthy tissues that is premalignant. Pancreatic acinar cells likely switch between edge and non-edge states, although the time spent by cells in either state is unclear. Establishing the stability of these states would require the tracing of lineages of acinar cells to infer the regulatory changes underlying the switching process.

Authors' Disclosures

No disclosures were reported.

Authors' Contributions

V. Gopalan: Conceptualization, data curation, software, formal analysis, investigation, visualization, methodology, writing–original draft, writing–review and editing. **A. Singh:** Data curation, software, formal analysis. **F.R. Mehrabadi:** Data curation, software, formal analysis. **L. Wang:** Formal analysis, validation, writing–review and editing. **E. Ruppin:** Investigation, writing–review and editing. **H.E. Arda:** Validation, writing–review and editing. **S. Hannenhalli:** Conceptualization, formal analysis, supervision, funding acquisition, investigation, visualization, methodology, writing–original draft, project administration, writing–review and editing.

Acknowledgments

References

1. Kleeff J, Korc M, Apte M, La Vecchia C, Johnson CD, Biankin AV, et al. Pancreatic cancer. Nat Rev Dis Primers 2016;2:16022.
2. Xu Y, Liu J, Nipper M, Wang P. Ductal vs. acinar? Recent insights into identifying cell lineage of pancreatic ductal adenocarcinoma. Ann Pancreat Cancer 2019;2:11.
3. Storz P. Acinar cell plasticity and development of pancreatic ductal adenocarcinoma. Nat Rev Gastroenterol Hepatol 2017;14:296–304.
4. Hanahan D, Weinberg RA. Hallmarks of cancer: the next generation. Cell 2011;144:646–74.
5. Nowell PC. The clonal evolution of tumor cell populations. Science 1976;194:23–8.
6. Feinberg AP, Ohlsson R, Henikoff S. The epigenetic progenitor origin of human cancer. Nat Rev Genet 2006;7:21–33.
7. Bernard V, Semaan A, Huang J, Lucas FAS, Mulu F, Stephens B, et al. Single-cell transcriptomics of pancreatic cancer precursors demonstrates epithelial and microenvironmental heterogeneity as an early event in neoplastic progression. Clin Cancer Res 2019;25:2194–205.
8. Hosein AN, Huang H, Wang Z, Parmar K, Du W, Huang J, et al. Cellular heterogeneity during mouse pancreatic ductal adenocarcinoma progression at single-cell resolution. JCI Insight 2019;5:e129212.
9. Thattai M, Van Oudenaarden A. Intrinsic noise in gene regulatory networks. Proc Natl Acad Sci U S A 2001;98:8614–9.
10. Chang HH, Hemberg M, Barahona M, Ingber DE, Huang S. Transcriptome-wide noise controls lineage choice in mammalian progenitor cells. Nature 2008;453:544–7.
11. Brock A, Chang H, Huang S. Non-genetic heterogeneity a mutation-independent driving force for the somatic evolution of tumours. Nat Rev Genet 2009;10:336–42.
12. Chaffer CL, Brueckmann I, Scheel C, Kaestli AJ, Wiggins PA, Rodrigues LO, et al. Normal and neoplastic nonstem cells can spontaneously convert to a stem-like state. Proc Natl Acad Sci U S A 2011;108:7950–5.
13. Vaz M, Hwang SY, Kagiampakis I, Phallen J, Patil A, O'Hagan HM, et al. Chronic cigarette smoke-induced epigenomic changes precede sensitization of bronchial epithelial cells to single-step transformation by KRAS mutations. Cancer Cell 2017;32:360–76.
14. Peng J, Sun BF, Chen CY, Zhou JY, Chen YS, Chen H, et al. Single-cell RNA-seq highlights intra-tumoral heterogeneity and malignant progression in pancreatic ductal adenocarcinoma. Cell Res 2019;29:725–38.
15. Li Q, Wennborg A, Aurell E, Dekel E, Zou JZ, Xu Y, et al. Dynamics inside the cancer cell attractor reveal cell heterogeneity, limits of stability, and escape. Proc Natl Acad Sci U S A 2016;113:2672–7.

16. Mascaux C, Angelova M, Vasaturo A, Beane J, Hijazi K, Anthoine G, et al. Immune evasion before tumour invasion in early lung squamous carcinogenesis. Nature 2019;571:570–5.

17. Aunan JR, Cho WC, Søreide K. The biology of aging and cancer: a brief overview of shared and divergent molecular hallmarks. Aging Dis 2017;8:628–42.

18. Kulakovskiy I, Levitsky V, Oshchepkov D, Bryzgalov L, Vorontsov I, Makeev V. From binding motifs in chip-seq data to improved models of transcription factor binding sites. J Bioinform Comput Biol 2013;11:1340004.

19. Fornes O, Castro-Mondragon JA, Khan A, Van Der Lee R, Zhang X, Richmond PA, et al. JASPAR 2020: update of the open-Access database of transcription factor binding profiles. Nucleic Acids Res 2020;48:D87–92.

20. Bauer AS, Nazarov PV, Giese NA, Beghelli S, Heller A, Greenhalf W, et al. Transcriptional variations in the wider peritumoral tissue environment of pancreatic cancer. Int J Cancer 2018;142:1010–21.

21. Stuart T, Butler A, Hoffman P, Hafemeister C, Papalexi E, Mauck WM, et al. Comprehensive integration of single-cell data. Cell 2019;177:1888–902.

22. McGinnis CS, Murrow LM, Gartner ZJ. DoubletFinder: doublet detection in single-cell RNA sequencing data using artificial nearest neighbors. Cell Syst 2019; 8:329–37.

23. Qiu X, Mao Q, Tang Y, Wang L, Chawla R, Pliner HA, et al. Reversed graph embedding resolves complex single-cell trajectories. Nat Methods 2017;14:979–82.

24. Baldan J, Houbracken I, Rooman I, Bouwens L. Adult human pancreatic acinar cells dedifferentiate into an embryonic progenitor-like state in 3D suspension culture. Sci Rep 2019;9:4040.

25. Puri S, Folias AE, Hebrok M. Plasticity and dedifferentiation within the pancreas: development, homeostasis, and disease. Cell Stem Cell 2015;16:18–31.

26. Pan FC, Bankaitis ED, Boyer D, Xu X, Van de Casteele M, Magnuson MA, et al. Spatiotemporal patterns of multipotentiality in Ptf1aexpressing cells during pancreas organogenesis and injury-induced facultative restoration. Development 2013;140:751–64.

27. Enge M, Arda HE, Mignardi M, Beausang J, Bottino R, Kim SK, et al. Single-cell analysis of human pancreas reveals transcriptional signatures of aging and somatic mutation patterns. Cell 2017;171:321–30.

28. Villani V, Thornton ME, Zook HN, Crook CJ, Grubbs BH, Orlando G, et al. SOX9+/PTF1A+ cells define the tip progenitor cells of the human fetal pancreas of the second trimester. Stem Cells Transl Med 2019;8:1249–64.

29. Aibar S, González-Blas CB, Moerman T, Huynh-Thu VA, Imrichova H, Hulselmans G, et al. SCENIC: single-cell regulatory network inference and clustering. Nat Methods 2017;14:1083–6.

30. Yuan H, Yan M, Zhang G, Liu W, Deng C, Liao G, et al. CancerSEA: a cancer single-cell state atlas. Nucleic Acids Res 2019;47:D900–8.

31. Arda HE, Tsai J, Rosli YR, Giresi P, Bottino R, Greenleaf WJ, et al. A chromatin basis for cell lineage and disease risk in the human pancreas. Cell Syst 2018;7: 310–22.

32. Arda HE, Benitez CM, Kim SK. Gene regulatory networks governing pancreas development. Dev Cell 2013;25:5–13.

33. He P, Yang JW, Yang VW, Bialkowska AB. Krüppel-like factor 5, increased in pancreatic ductal adenocarcinoma, promotes proliferation, acinar-to-ductal metaplasia, pancreatic intraepithelial neoplasia, and tumor growth in mice. Gastroenterology 2018;154:1494–508.

34. Hidalgo-Sastre A, Brodylo RL, Lubeseder-Martellato C, Sipos B, Steiger K, Lee M, et al. Hes1 controls exocrine cell plasticity and restricts development of pancreatic ductal adenocarcinoma in a mouse model. Am J Pathol 2016;186: 2934–44.

35. Muraro MJ, Dharmadhikari G, Grün D, Groen N, Dielen T, Jansen E, et al. A single-cell transcriptome atlas of the human pancreas. Cell Syst 2016;3:385–94.

36. Yizhak K, Aguet F, Kim J, Hess JM, Kübler K, Grimsby J, et al. RNA sequence analysis reveals macroscopic somatic clonal expansion across normal tissues. Science 2019;364:eaaw0726.

37. Liu F, Zhang Y, Zhang L, Li Z, Fang Q, Gao R, et al. Systematic comparative analysis of single-nucleotide variant detection methods from single-cell RNA sequencing data. Genome Biol 2019;20:242.

38. Sondka Z, Bamford S, Cole CG, Ward SA, Dunham I, Forbes SA. The COSMIC Cancer Gene Census: describing genetic dysfunction across all human cancers. Nat Rev Cancer 2018;18:696–705.

39. Sutherland KD, Song JY, Kwon MC, Proost N, Zevenhoven J, Berns A. Multiple cells-of-origin of mutant K-Ras–induced mouse lung adenocarcinoma. Proc Natl Acad Sci U S A 2014;111:4952–7.

40. Kim N, Kim HK, Lee K, Hong Y, Cho JH, Choi JW, et al. Single-cell RNA sequencing demonstrates the molecular and cellular reprogramming of metastatic lung adenocarcinoma. Nat Commun 2020;11:2285.

41. MacParland SA, Liu JC, Ma XZ, Innes BT, Bartczak AM, Gage BK, et al. Single cell RNA sequencing of human liver reveals distinct intrahepatic macrophage populations. Nat Commun 2018;9:4383.

42. Ma L, Hernandez MO, Zhao Y, Mehta M, Tran B, Kelly M, et al. Tumor cell biodiversity drives microenvironmental reprogramming in liver cancer. Cancer Cell 2019;36:418–30.

43. Smillie CS, Biton M, Ordovas-Montanes J, Sullivan KM, Burgin G, Graham DB, et al. Intra- and inter-cellular rewiring of the human colon during ulcerative colitis. Cell 2019;178:714–30.

44. Qian J, Olbrecht S, Boeckx B, Vos H, Laoui D, Etlioglu E, et al. A pan-cancer blueprint of the heterogeneous tumor microenvironment revealed by single-cell profiling. Cell Res 2020;30:745–62.

45. Karthaus WR, Hofree M, Choi D, Linton EL, Turkekul M, Bejnood A, et al. Regenerative potential of prostate luminal cells revealed by single-cell analysis. Science 2020;368:497–505.

46. Yadav D, Lowenfels AB. The epidemiology of pancreatitis and pancreatic cancer. Gastroenterology 2013;144:1252–61.

47. Tosti L, Hang Y, Debnath O, Tiesmeyer S, Trefzer T, Steiger K, et al. Single-nucleus and in situ RNA-sequencing reveal cell topographies in the human pancreas. Gastroenterology 2021;160:1330–44.

48. Fukuda A, Wang SC, Morris JP, Folias AE, Liou A, Kim GE, et al. Stat3 and MMP7 contribute to pancreatic ductal adenocarcinoma initiation and progression. Cancer Cell 2011;19:441–55.

49. Jakubowska K, Pryczynicz A, Januszewska J, Sidorkiewicz I, Kemona A, Niewiński A, et al. Expressions of matrix metalloproteinases 2, 7, and 9 in carcinogenesis of pancreatic ductal adenocarcinoma. Dis Markers 2016;2016: 9895721.

50. Kuhlmann KFD, Van Till JWO, Boermeester MA, De Reuver PR, Tzvetanova ID, Offerhaus GJA, et al. Evaluation of matrix metalloproteinase 7 in plasma and pancreatic juice as a biomarker for pancreatic cancer. Cancer Epidemiol Biomarkers Prev 2007;16:886–91.

51. Jones LE, Humphreys MJ, Campbell F, Neoptolemos JP, Boyd MT. Comprehensive analysis of matrix metalloproteinase and tissue inhibitor expression in pancreatic cancer: increased expression of matrix metalloproteinase-7 predicts poor survival. Clin Cancer Res 2004;10:2832–45.

52. Waters AM, Der CJ. KRAS: the critical driver and therapeutic target for pancreatic cancer. Cold Spring Harb Perspect Med 2018;8:a031435.

53. Schaum N, Karkanias J, Neff NF, May AP, Quake SR, Wyss-Coray T, et al. Single-cell transcriptomics of 20 mouse organs creates a Tabula Muris. Nature 2018;562: 367–72.

54. Almanzar N, Antony J, Baghel AS, Bakerman I, Bansal I, Barres BA, et al. A single-cell transcriptomic atlas characterizes ageing tissues in the mouse. Nature 2020;583:590–5.

55. Schlesinger Y, Yosefov-Levi O, Kolodkin-Gal D, Granit RZ, Peters L, Kalifa R, et al. Single-cell transcriptomes of pancreatic preinvasive lesions and cancer reveal acinar metaplastic cells' heterogeneity. Nat Commun 2020; 11:4516.

56. Cobo I, Martinelli P, Flández M, Bakiri L, Zhang M, Carrillo-De-Santa-Pau E, et al. Transcriptional regulation by NR5A2 links differentiation and inflammation in the pancreas. Nature 2018;554:533–7.

57. Fazio EN, Young CC, Toma J, Levy M, Berger KR, Johnson CL, et al. Activating transcription factor 3 promotes loss of the acinar cell phenotype in response to cerulein-induced pancreatitis in mice. Mol Biol Cell 2017;28: 2347–59.

58. Li X, Lin Z, Wang L, Liu Q, Cao Z, Huang Z, et al. RNA-Seq analyses of the role of miR-21 in acute pancreatitis. Cell Physiol Biochem 2018;51: 2198–211.

59. DelGiorno KE, Naeem RF, Fang L, Chung CY, Ramos C, Luhtala N, et al. Tuft cell formation reflects epithelial plasticity in pancreatic injury: implications for modeling human pancreatitis. Front Physiol 2020;11:88.

60. Alonso-Curbelo D, Ho YJ, Burdziak C, Maag JLV, Morris JP, Chandwani R, et al. A gene–environment-induced epigenetic program initiates tumorigenesis. Nature 2021;590:642–8.

61. Huang S. Non-genetic heterogeneity of cells in development: More than just noise. Development 2009;136:3853–62.

62. Shaffer SM, Dunagin MC, Torborg SR, Torre EA, Emert B, Krepler C, et al. Rare cell variability and drug-induced reprogramming as a mode of cancer drug resistance. Nature 2017;546:431–5.

63. Emert BL, Coté C, Torre EA, Dardani IP, Jiang CL, Jain N, et al. Variability within rare cell states enables multiple paths towards drug resistance. Nat Biotechnol 2021Feb 22. [Epub ahead of print].

64. Bird A. DNA methylation patterns and epigenetic memory. Genes Dev 2002;16: 6–21.

65. Dodd IB, Micheelsen MA, Sneppen K, Thon G. Theoretical analysis of epigenetic cell memory by nucleosome modification. Cell 2007;129:813–22.

66. Siegel RL, Miller KD, Jemal A. Cancer statistics, 2020. CA Cancer J Clin 2020;70: 7–30.

67. Martincorena I. Somatic mutation and clonal expansions in human tissues. Genome Med 2019;11:35.

68. Horvath S. DNA methylation age of human tissues and cell types. Genome Biol 2013;14:R115.

69. Hinkal G, Parikh N, Donehower LA. Timed somatic deletion of p53 in mice reveals age-associated differences in tumor progression. PLoS ONE 2009;4: e6654.

70. Tao Y, Kang B, Petkovich DA, Bhandari YR, In J, Stein-O'Brien G, et al. Aging-like spontaneous epigenetic silencing facilitates Wnt activation, stemness, and Braf V600E–induced tumorigenesis. Cancer Cell 2019;35:315–28.